

On the coupled response to ice-shelf basal melting

Christopher M. LITTLE,¹ Daniel GOLDBERG,² Anand GNANADESIKAN,³
Michael OPPENHEIMER^{1,4}

¹Woodrow Wilson School of Public and International Affairs, Princeton University, Princeton, NJ, USA
E-mail: cmlittle@princeton.edu

²Department of Earth, Atmospheric and Planetary Sciences, Massachusetts Institute of Technology,
Cambridge, MA, USA

³Department of Earth and Planetary Sciences, Johns Hopkins University, Baltimore, MD, USA

⁴Department of Geosciences, Princeton University, Princeton, NJ, USA

ABSTRACT. Ice-shelf basal melting is tightly coupled to ice-shelf morphology. Ice shelves, in turn, are coupled to grounded ice via their influence on compressive stress at the grounding line ('ice-shelf buttressing'). Here, we examine this interaction using a local parameterization that relates the basal melt rate to the ice-shelf thickness gradient. This formulation permits a closed-form solution for a steady-state ice tongue. Time-dependent numerical simulations reveal the spatial and temporal evolution of ice-shelf/ice-stream systems in response to changes in ocean temperature, and the influence of morphology-dependent melting on grounding-line retreat. We find that a rapid (<1 year) re-equilibration in upstream regions of ice shelves establishes a spatial pattern of basal melt rates (relative to the grounding line) that persists over centuries. Coupling melting to ice-shelf shape generally, but not always, increases grounding-line retreat rates relative to a uniform distribution with the same area-average melt rate. Because upstream ice-shelf thickness gradients and retreat rates increase nonlinearly with thermal forcing, morphology-dependent melting is more important to the response of weakly buttressed, strongly forced ice streams grounded on beds that slope upwards towards the ocean (e.g. those in the Amundsen Sea).

INTRODUCTION

Several regions of the Antarctic ice sheet have lost mass over the last decade (Rignot and others, 2008; Pritchard and others, 2009; Wu and others, 2010; Zwally and Giovinetto, 2011), with the largest losses observed in the Amundsen Sea sector (Shepherd and Wingham, 2007; Rignot, 2008). Because thinning has been observed to originate on ice shelves and propagate up-glacier (Pritchard and others, 2009; Scott and others, 2009), as predicted by numerical simulations of ice streams subject to a perturbation at their termini (Schmeltz and others, 2002; Payne and others, 2004; Thomas, 2004; Dupont and Alley, 2005; Nick and others, 2009), increases in ice-shelf basal melting have been invoked as the underlying 'trigger' for ice loss (e.g. Payne and others, 2004). If sustained over centuries, higher melt rates could result in large changes in the mass and extent of the Antarctic ice sheet (Pollard and DeConto, 2009). Clarifying the linkage between decadal- and century-timescale ice losses (and thus changes in sea level) requires an understanding of the persistence of oceanic changes, the timescales of glaciological response and any internal feedbacks in the coupled response of the ice/ocean system. Here we focus on the latter two problems, highlighting the glaciological impact of the co-evolution of ice-shelf morphology and basal melting.

Without guidance from numerical models, glaciological and oceanographic observations cannot define a precise chain of events underlying recent thinning. Although ocean temperatures and basal melt rates are higher in the Amundsen Sea than elsewhere in Antarctica (Jacobs and others, 1996; Rignot and Jacobs, 2002), and recent increases in basal melting have been attributed to increased ocean heat content (Rignot and others, 2008; Thoma and others, 2008;

Jacobs and others, 2011), historical ocean data documenting a long-term warming trend are lacking. Even if a record were available, it is not clear how large, or how sustained, changes in ocean temperatures need to be to drive morphological changes and grounding-line retreat. An evolving ice shelf complicates the observational linkage between oceanic change and glaciological impacts. Simultaneous changes in ice thickness, velocity and grounding-line position (Rignot, 2008; Wingham and others, 2009) convolve historical changes in the ocean or ice with the ongoing evolution of basal melting and the glaciological stress regime (Jenkins and others, 2010; Jacobs and others, 2011).

The response of grounded ice to ocean temperature may also be modified by internal ice/ocean feedbacks. In particular, following an increase in ocean temperature, steepening ice-shelf basal slopes may enhance the turbulent transport of heat from the interior ocean to the ice/ocean boundary, increasing the area-average basal melt rate or shifting its distribution (Holland and Jenkins, 1999; Walker and Holland, 2007; Little and others, 2009). Model simulations with constant basal melt rates (Walker and others, 2008; Gagliardini and others, 2010), constant ice-shelf thickness (Holland and others, 2008; Little and others, 2009) or constant grounding-line position (Holland and Jenkins, 1999; Walker and Holland, 2007; Little and others, 2009) imply that this slope-dependent (here also referred to as 'morphology-dependent' or 'coupled') melting response is likely to enhance ice loss.

To capture these coupled processes, models must represent the (presumably rapid) spatial and temporal evolution of basal melting and its long-term influence on grounded ice. Parizek and Walker (2010) made progress in this direction, passing melt rates derived from a steady-state ocean plume

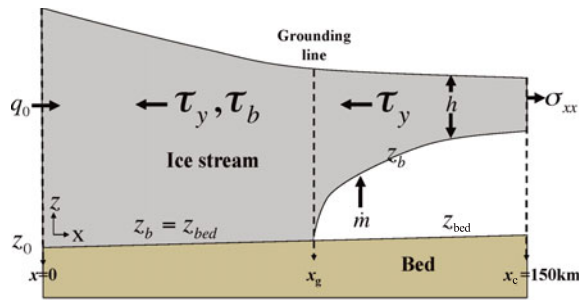


Fig. 1. Schematic illustration of the numerical simulations. In this paper, the velocity, u , and thickness, h , of an ice stream are calculated using a vertically integrated flowline model subject to an upstream input flux, q_0 , basal melting, \dot{m} , where ice is floating, and a downstream stress boundary condition, σ_{xx} . All other variables are defined in Table 1.

model to an ice-stream/ice-shelf model. Changes in the melt rate and its distribution are a strong function of the local basal slope of the ice shelf and act to increase grounding-line retreat. However, short-timescale (<5 years) changes in melt rates were not resolved, and the results were sensitive to bedrock topography.

In this study, we permit rapid (<1 month) changes in basal melting and examine their influence on grounding-line position over a range of glaciological settings. Numerical simulations are conducted using a vertically integrated ice-stream model (shown schematically in Fig. 1). The distributional effect of a coupled melt rate is isolated with ‘uniform’ simulations that utilize a constant, spatially uniform melt rate.

Key aspects of the morphological evolution of ice shelves can be interpreted using ‘unbuttressed’ simulations that do not include lateral stresses. Simulations that include lateral stresses reveal the influence of melt-induced thinning on grounding-line retreat and the dependence of the coupled system on ice-stream geometry. By tracing the evolution of local melt rates, ice-shelf shape and grounding-line retreat, we determine when the coupled response is important. This analysis informs the interpretation of previous modeling studies, the attribution of observed glaciological changes to the ocean and the design of more comprehensive and realistic coupled land-ice/ocean models.

GOVERNING EQUATIONS AND NUMERICAL MODEL

Ice-stream/ice-shelf model

The behavior of an ice-shelf/ice-stream system may be approximated using the shallow-shelf approximation (MacAyeal, 1989) in one dimension, where the stress balance is given by (after Dupont, 2004)

$$\partial_x \left(4h\nu\partial_x u - \frac{\rho_i g}{2} h^2 \right) = \rho_i g h \partial_x z_b + \tau_y + \begin{cases} \langle \tau_b \rangle_y & \text{grounded} \\ 0 & \text{floating} \end{cases} \quad (1)$$

In Eqn (1), u is the ice velocity in the along-flow dimension, x , h is the ice thickness, g is gravitational acceleration, τ_b and τ_y are basal and lateral stresses, z_b is the basal elevation, ρ_i and ρ_w are the mean (constant) densities of the ice shelf and sea water, and angle brackets indicate width-averaging.

Table 1. Variables used in the text, and parameters employed in numerical simulations. All quantities with overbars are given by $\overline{[]}(t) = [x - x_g]^{-1} \int_{x_g}^x [] dx$. All primed quantities indicate perturbations from an initial state denoted by subscript 0

Parameter	Symbol	Unit	Numeric value
Distance	x	m	
Ice velocity	u	m s^{-1}	
Ice thickness	h	m	
Time	t	s	
Basal melt rate	\dot{m}	m s^{-1}	
Ice-shelf basal slope	θ		
Lateral stress	τ_y	Pa	
Basal stress	τ_b	Pa	
Effective viscosity	ν	Pa s	
Basal melting coefficient	a_b	m s^{-1}	
Ocean forcing parameter	α		
Ice flux at $x = 0$	q_0	$\text{m}^2 \text{s}^{-1}$	
Width parameter	W	m	
Bed elevation	z_{bed}	m	
Basal elevation	z_b	m	
Length of ice shelf	L_x	m	
Buttressing parameter	f		
f at grounding line	f_g		
Grounding-line position	x_g	m	
Grounding-line migration rate	\dot{x}_g	m s^{-1}	
Ice velocity at grounding line	u_g	m s^{-1}	
Ice thickness at grounding line	h_g	m	
Glen’s law coefficient	A	$\text{Pa}^{-3} \text{s}^{-1}$	4.9×10^{-25}
Basal drag coefficient	C	$\text{Pa m}^{-1} \text{s}$	1×10^9
Ice density	ρ_i	kg m^{-3}	917
Ocean density	ρ_w	kg m^{-3}	1028
Gravitational acceleration	g	m s^{-2}	9.8
Exponent in flow law	n		3
Length of domain	L	m	1.5×10^5
Downstream domain boundary	x_c	m	1.5×10^5
Basal melting slope sensitivity	n_θ		1

The effective viscosity of ice, ν , is

$$\nu = \frac{A^{\frac{1}{n}}}{2} |\partial_x u|^{\frac{1-n}{n}} \quad (2)$$

where A and n are the (constant) flow law parameter and exponent, respectively (Paterson, 2001, ch. 5). Without surface accumulation, the ice thickness evolution is governed by

$$\partial_t h = -\partial_x (uh) - \dot{m} \quad (3)$$

The flowline model described by Goldberg and others (2009) is used to solve Eqns (1) and (3) on a 150 km domain with an adaptive mesh of 500 gridpoints, subject to a constant upstream input flux of ice, q_0 , and basal melting, \dot{m} (Fig. 1). The bed elevation is given by:

$$z_{\text{bed}} = z_{\text{bed}}(x=0) + \partial_x z_{\text{bed}} x \quad (4)$$

where $\partial_x z_{\text{bed}}$ is constant over the domain. Variables used in this paper, and the values of parameters held constant through all simulations, are listed in Table 1.

For an ice shelf in hydrostatic equilibrium

$$z_b = -\frac{\rho_i}{\rho_w} h \quad (5)$$

ice floats if the ocean pressure can support the ice column (e.g. where $z_b > z_{\text{bed}}$). The grounding-line position, x_g , is linearly interpolated between the first floating and last grounded gridpoints. A stress boundary condition is applied

Table 2. Glaciological parameters that are varied between simulations to achieve a 50 km long non-melting ice shelf. The naming convention is as follows: U(D) indicates an upward-sloping (downward-sloping) bed; the number indicates the value of the buttressing parameter before the initiation of melting

Parameter	Symbol	U50	U75	D50	D75	D00	Unit
Bed slope	$\partial_x z_{\text{bed}}$	3.0	3.0	-3.0	-3.0	-3.0	$\times 10^{-3}$
Bed elevation at upstream boundary	$z_{\text{bed}}(x = 0)$	-1191	-1191	-443	-443	-443	m
Width scale	W	30.25	15.5	34.4	21.0	∞	km
Ice flux at upstream boundary	q_0	2.39	0.58	1.78	0.78	4.57	$\text{km}^2 \text{a}^{-1}$

at the downstream boundary of the domain, x_c , presumed to be a stationary calving front, where:

$$\left[4h\nu\partial_x u - \frac{\rho_i g}{2} h^2\right]_{x=x_c} = -\left[\frac{\rho_w g}{2} z_b^2\right]_{x=x_c} \quad (6)$$

At x_c the calving rate is equal to the ice velocity.

A linear-viscous basal drag is imposed on grounded ice:

$$\tau_b = -Cu \quad (7)$$

Lateral stress is parameterized after Dupont (2004):

$$\tau_y = \frac{2hu^{\frac{1}{3}}}{W^{\frac{4}{3}}} \quad (8)$$

where W is a width scale. At any point on the ice shelf, a ‘buttressing parameter’ may be expressed as (Walker and others, 2008)

$$f = \frac{\int_x^{x_c} \tau_y dx}{\left[\rho_i g \left(1 - \frac{\rho_i}{\rho_w}\right)\right] h^2} \quad (9)$$

The fraction of the driving stress at the grounding line balanced by lateral stress in the ice shelf is given by $f_g = f(x_g)$.

Basal melting parameterization

Little and others (2009) discuss a melting parameterization of the form:

$$\dot{m} = a_b(\theta, T)\theta^{n_\theta(\theta, T)} \quad (10)$$

where θ is the local slope of the spatially and temporally varying basal elevation of the ice shelf ($\|\nabla z_b(x, y, t)\|$), and T is the ‘far-field’ or ‘interior’ ocean temperature. Although a_b may depend nonlinearly on temperature (Holland and others, 2008), temperature and slope dependence are not completely separable, and n_θ is spatially variable (Little and others, 2009), a simplified form of Eqn (10) is sufficient to illustrate the impact of a time-varying, slope-dependent melt rate on the glaciological response. We thus assume that $n_\theta = 1$, and examine the response to linear stepwise changes in a_b (‘ocean forcing’) without examining the details of the implied temperature dependence.

The sea-water freezing point is not explicitly included in Eqn (10). However, where ocean temperatures are higher than the surface freezing point (as in the Amundsen Sea), gradients in melting driven by slope are likely to dominate those arising from the freezing point, and pressure dependence may be compensated by salinity within the ocean boundary layer (Little and others, 2009). Eqn (10) is unlikely to be adequate where subsurface water is close to the surface freezing point (e.g. under the Ross Ice Shelf) or where tidal processes are dominant.

Along a flowline, using Eqns (5) and (10), basal melting can be written in terms of the ice-shelf thickness gradient and the grounding-line velocity so that:

$$\dot{m} = -\alpha u_g |\partial_x h| \quad (11)$$

where u_g is the ice velocity at the grounding line, and $0 \leq \alpha < 1$. The ocean forcing parameter, α , is used to compare the impact of perturbations in basal melting that result in similar integrated mass loss for different ice streams, highlighting the influence of the glaciological stress regime on the ice-shelf shape and the melting distribution. To prevent unbounded melt rates in the numerical simulations:

$$\dot{m} = -\alpha u_g \frac{|\partial_x h|}{1 + |\partial_x h|} \quad (12)$$

for each gridpoint on which ice is fully floating. The local and spatially averaged basal melt rates change with time and with α .

Experimental design

We perform simulations with two values of f_g , two different bed slopes, and two forms of melting (‘coupled’ and ‘uniform’). To achieve a specified f_g for the initial, non-melting state, q_0 and W are adjusted to achieve $L_x(t = 0) = 50 \text{ km}$ (Table 2). Where $\partial_x z_{\text{bed}} = 3.0 \times 10^{-3}$ and $f_g(t = 0) = 0.50$, the parameters (and resulting ice-stream shape and velocity structure) are similar to those of Walker and others (2008). This simulation is denoted as the U50 case, where U indicates an upward-sloping ($\partial_x z_{\text{bed}} > 0$) bed, and the number indicates f_g before melting is initiated. This setting more faithfully represents observations of ice-shelf and bedrock morphology in the Amundsen Sea sector (Vaughan and others, 2006; Jenkins and others, 2010) than other simulations.

Each simulation is integrated for 600 years, by which time grounding-line migration, \dot{x}_g , is less than $O(10^{-5} \text{ ma}^{-1})$; ice thickness and melt rates are presumed to be steady. Successive step changes in ocean forcing ($\Delta\alpha = 0.25$) are applied up to an end point that depends on the bedrock slope: $\partial_x z_{\text{bed}} > 0$, when the grounding line retreats unstably; $\partial_x z_{\text{bed}} < 0$, when the ice thickness gradient anywhere on the domain is > 0.1 . The final melt rates for the coupled U50 simulations are shown along with surface, basal and bed elevations in Figure 2.

For each coupled simulation that reaches a steady state, the spatially averaged melt rate over the ice shelf is calculated:

$$\bar{\dot{m}} = \frac{\int_{x_g}^{x_c} \dot{m}(t = 600) dx}{L_x(t = 600)} \quad (13)$$

The simulation is then rerun from its initial state using the spatially and temporally constant value in Eqn (13).

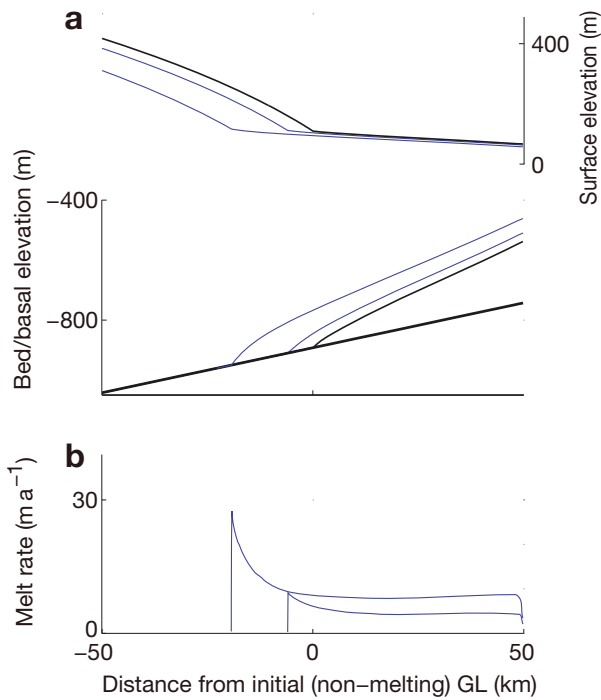


Fig. 2. An example of the coupled evolution of melting and morphology. Final profiles of (a) surface (thin lines, right axis), basal (thin lines, left axis) and bed elevations (thick line, left axis) and (b) basal melt rates, after step changes to $\alpha = 0.25$ (dotted gray lines) and $\alpha = 0.50$ (solid gray lines), in the coupled U50 simulation. Here, $x = 50$ corresponds to x_c . Non-melting ice-stream profiles are shown with black lines. GR is grounding line.

RESULTS

Our results present: (1) common features and timescales in the co-evolution of melting and ice-shelf thickness; (2) the linkage between the ice-shelf thickness evolution and grounding-line retreat; and (3) the implications of these more general results in other glaciological settings.

Ice-stream response timescales

Although there is no dynamic linkage between an ice shelf and grounded ice in the D00 ('unbuttressed') simulations (Schoof, 2007), steady-state solutions for ice-shelf thickness provide insight into the local sensitivity of melt rates and thinning to ocean forcing (Appendix A). The establishment and propagation of a melting signature may also be interpreted using a simplified set of ice-shelf-only equations.

Without basal or lateral stresses, Eqn (1) may be used to describe a depth-integrated, free-floating ice shelf:

$$\partial_x u = \left[\frac{\rho_i g}{4} \left(1 - \frac{\rho_i}{\rho_w} \right) \right]^n A h^n \quad (14)$$

The evolution of ice-shelf thinning in response to melting can be interpreted by substituting Eqn (14) into Eqn (3):

$$-\partial_t h = u \partial_x h + \left[\frac{\rho_i g}{4} \left(1 - \frac{\rho_i}{\rho_w} \right) \right]^n A h^{n+1} + \dot{m} \quad (15)$$

Linearizing Eqn (15) about a melting perturbation, \dot{m}' :

$$\begin{aligned} -\partial_t (h_0 + h') &= (u_0 + u') \partial_x (h_0 + h') \\ &+ \left[\frac{\rho_i g}{4} \left(1 - \frac{\rho_i}{\rho_w} \right) \right]^n A (h_0 + h')^{n+1} \\ &+ \dot{m}_0 + \dot{m}' \end{aligned} \quad (16)$$

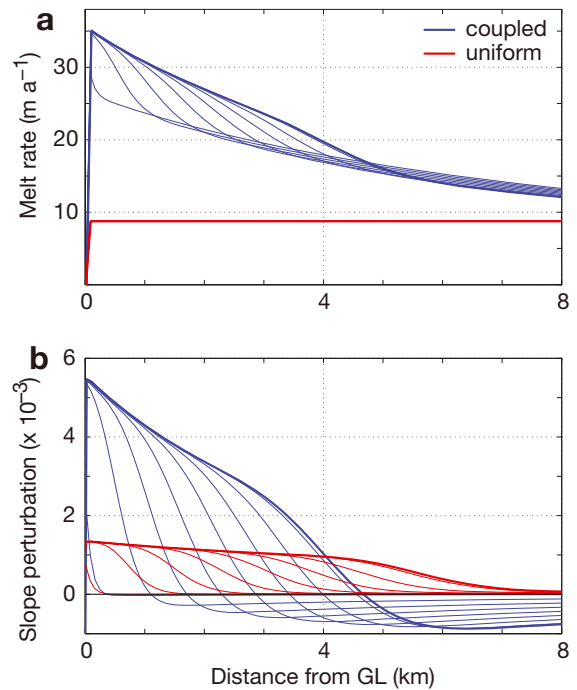


Fig. 3. Initiation of the slope wave. Instantaneous profiles of perturbations from initial values of (a) basal melting, \dot{m}' , and (b) basal slope, $-\frac{\rho_i}{\rho_w} \partial_x h'$, at 50 day intervals after initiation of melting in an unbuttressed ice shelf (only the first 8 km seaward of the grounding line are shown). Values at $t = 1$ year are shown with thick curves. The coupled simulation ($\alpha = 0.25$) is shown as blue curves; the uniform simulation is shown in red. Here $\dot{m} = \dot{m}'$; subsequent increases in α share the same features. GL is grounding line.

If only the lowest-order terms in h_0 are retained, the steady balance is removed and the velocity perturbation is assumed to be small, $(u'/u_0) \ll (\partial_x h'/\partial_x h_0)$, then Eqn (16) becomes

$$-\partial_t h' = u_0 \partial_x h' + (n + 1) \left[\frac{\rho_i g}{4} \left(1 - \frac{\rho_i}{\rho_w} \right) \right]^n A h_0^n h' + \dot{m}' \quad (17)$$

Subject to these approximations, increases in melting ($\dot{m}' > 0$) induce thinning ($-\partial_t h' > 0$) at a rate that is lessened by reductions in stretching stress ($h' < 0$) and/or increases in ice flux convergence ($\partial_x h' < 0$).

When a uniform melt rate is imposed on an unbuttressed ice shelf (red curves in Fig. 3a), thinning downstream of the grounding line (which does not change position) initiates a large change in the ice thickness gradient. Near the grounding line, \dot{m}' is compensated rapidly and almost entirely by $u_0 \partial_x h'$; the final ice thickness is attained within months of the change in melt rate (Fig. 3b). Advection of this large perturbation in the thickness gradient drives an enhancement of basal slope that propagates downstream at the ice velocity ($u_g \approx 5.5 \text{ km a}^{-1}$), allowing the establishment of a new local equilibrium to the changed melt rate (Walker and Holland, 2007).

The coupled simulation (blue curves in Fig. 3) develops gradients in thinning due to spatially and temporally varying melt rates; where initial ice thickness gradients are weak (downstream), melting drives a transient relaxation in basal slope. Yet the dominant morphological signal remains the propagation of a wave with its origins in the glaciological response; its larger magnitude in the coupled simulation is

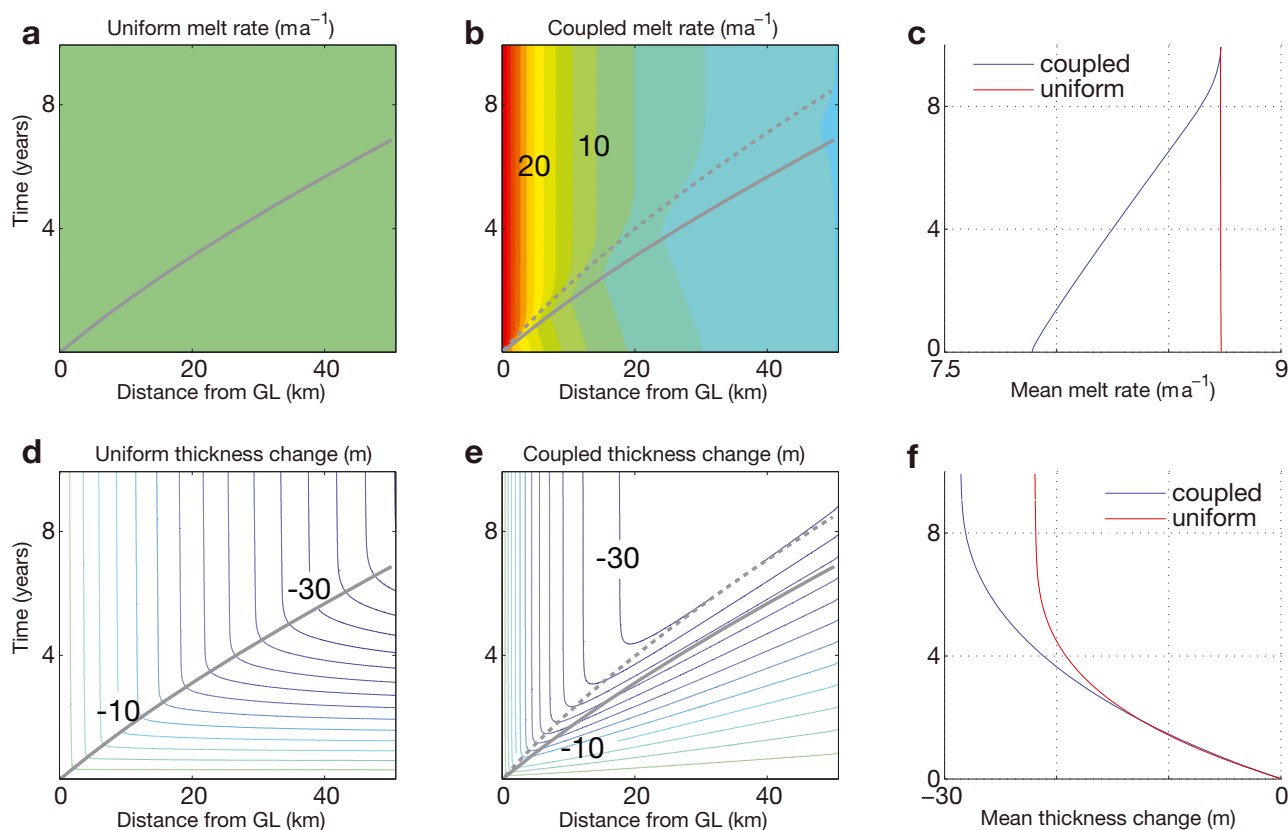


Fig. 4. Morphological evolution of an unbuttressed ice shelf subject to a step change in ocean forcing. Melting rates (\bar{m} ; a–c) and ice-shelf thickness perturbations (h' ; d–f) resulting from uniform (a, d) and coupled (b, e; $\alpha = 0.25$) melting imposed on an initially non-melting ice shelf (as in Fig. 3). The solid gray line represents the path of ice initially at the grounding line traveling at the unperturbed ice velocity, $u(x, t=0)$; in (b) and (e) the dotted gray line shows the path of ice traveling at $u(x, t=0) - \alpha u_g$. (c, f) The evolution of mean ice-shelf quantities for coupled (blue) and uniform (red) melting. (c) The evolution of the spatially averaged melt rate, \bar{m} , and (f) the mean shelf-averaged thickness perturbation, $\bar{h}'(t)$. GL is grounding line.

driven by high melt rates acting on ice thickness gradients (not by spatial gradients in the melt rate).

As expected from Eqn (17), re-equilibration to a melting perturbation occurs over the ice-shelf advective timescale (see also MacAyeal and Barcilon, 1988). The local adjustment to a spatially uniform melt rate stops as the slope wave passes (Fig. 4d), following a characteristic that originates at the grounding line; thinning persisting after the wave passage is due principally to the ignorance of velocity perturbations in Eqn (17). Adjustment to changed ocean forcing is complete after this wave reaches the calving front.

In the coupled simulation, melt rates adjust to changing ice thickness gradients. Because \bar{m} increases toward its final value, the characteristic time derivative in Eqn (17) is initially smaller (and the adjustment timescale is longer) than if melt rates were held constant at their final values. With the melting parameterization employed here, the coupled evolution effectively slows the advective process driving re-equilibration:

$$-\partial_t h = (u - \alpha u_g) \partial_x h + h \partial_x u \quad (18)$$

The deviation from the wave speed predicted by Eqn (18) (dotted curve in Fig. 4e) is due to upstream-weighted thinning reducing the driving stress, and thus lowering velocities, everywhere in the ice shelf.

Changes in the area-averaged melt rate are dominated by the initial, rapid re-equilibration of upstream sections of the ice shelf (Fig. 4c); ongoing steepening results in a relatively

small change in the mean melt rate ($\sim 10\%$). However, the mean thinning rate (and the rate of reduction in the sidewall area of the ice shelf, where grounding-line and calving-front positions are fixed) is driven by the downstream propagation of this initial thickness adjustment (Fig. 4f). After this thinning signal propagates through the ice shelf, the ice-shelf sidewall area of the coupled simulation is reduced by an additional 30% relative to the uniform melt rate. The additional thinning due to morphology-dependent melting increases with α (Appendix A).

In ‘buttressed’ ice shelves ($f_g > 0$), lateral stress does not qualitatively alter the down-glacier evolution of ice thickness; Eqn (3) continues to govern the timescales over which melting distributions induce thinning (see also MacAyeal and Lange, 1988). Over the advective timescale of the ice shelf (~ 20 years), the propagation of a slope wave in the U50 simulations is analogous to the unbuttressed simulations (lower panels of Fig. 5a and b). With uniform melting, local basal slopes steepen until the arrival of the signal originating at the grounding line. In the coupled simulations, a large initial adjustment establishes the melt rate in upstream regions; downstream relaxation of ice thickness gradients is followed by steepening and re-equilibration.

Buttressed ice shelves are characterized by a second, longer, timescale as the grounding line migrates inland. The century-timescale thickness evolution consists of an upstream translation of the (steepened) ice shelf: basal slope remains approximately constant with distance from the

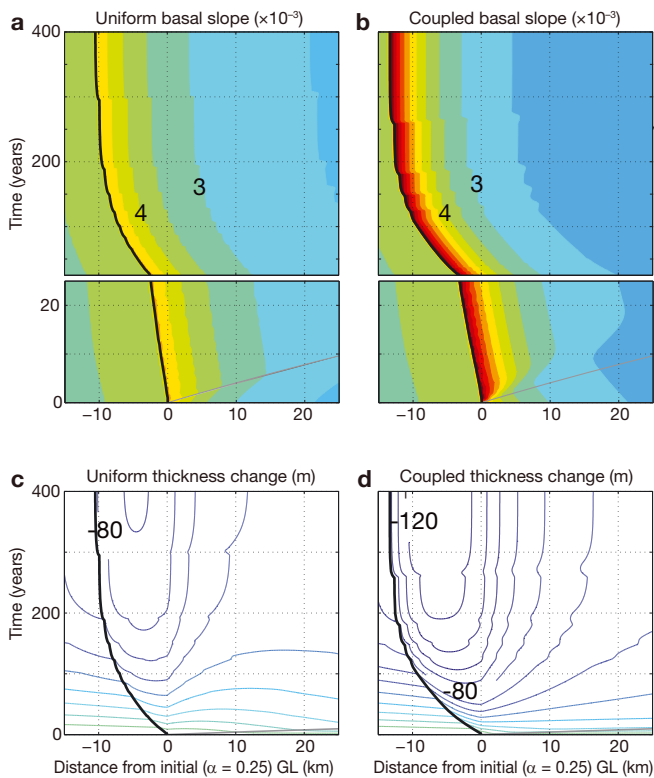


Fig. 5. Morphological evolution of the U50 simulation. Basal slope (a, b; $-10^3 \frac{\rho_i}{\rho_w} \partial_x h'$) and ice thickness (c, d; h') perturbations resulting from a step change in α from 0.25 to 0.50, with uniform (a, c) and coupled (b, d) melting. In the lower panels of (a) and (b) a different scale highlights the evolution of basal slope over the first 25 years of the simulations; as in Figure 4, the gray curve illustrates the path of ice at the grounding line traveling at the initial ice velocity. In all panels, the thick black curve describes the grounding-line trajectory in x - t space. Only a 40 km window around the grounding line is shown. GL is grounding line.

grounding line (upper panels of Fig. 5a and b). Flotation of formerly grounded ice does not substantially change basal slope near the grounding line; changes in u_g and h_g are small and slower than the initial change in melt rates following a change in α . The coupled ice shelf thus remains thinner than the uniform simulation despite a deeper grounding line (Fig. 5c and d).

The role of morphology-dependent melting in grounding-line retreat

The two timescales of ice thickness evolution evident in Figure 5 are linked by the co-evolution of lateral stresses in the ice shelf and the grounding-line position. Here we highlight the mechanisms by which morphology-dependent melting modifies the rate of grounding-line retreat, and the timescales over which its impacts manifest, using the U50 simulations as an example. Other buttressed simulations share the same underlying dynamics, and are discussed in the following subsection to illustrate the interaction of ice-shelf shape, bedrock slope and grounding-line retreat.

As shown in Appendix B, in this regime the grounding-line stretching tendency controls the rate of retreat and the return to a stable position. If $n = 3$,

$$-\dot{x}_g \sim h_g^4 (1 - f_g)^3 \quad (19)$$

Using Eqns (19), (9) and (8),

$$-\dot{x}_g \sim h_g^4 \left[1 - \frac{2 \int_{x_g}^{x_g+L_x(t)} h u^{\frac{1}{3}} dx}{\rho_i g \left(1 - \frac{\rho_i}{\rho_w}\right) W^{\frac{4}{3}} h_g^2} \right]^3 \quad (20)$$

The grounding-line retreat rate, $-\dot{x}_g$, is increased by ice-shelf thinning, h , decreased by the extension of the ice shelf upon retreat, $L_x(t)$, and either reduced or increased by ice thickness at the grounding line, h_g , which is a function of the sign of the bedrock slope; these controls determine when the coupled response influences buttressing and retreat rates.

The first 40 years of the U50 simulations is characterized by a shift in importance from melting-induced changes in ice-shelf morphology to bed morphology (Fig. 6a and b). Initially, the grounding-line response is driven by ice-shelf thinning, but the retreat rate is only weakly dependent upon the melting distribution; differences in the sidewall area must evolve (as in Fig. 4f). As thickness changes resulting from the melting distribution are advected downstream, changing the sidewall area, differences in f_g and \dot{x}_g increase in tandem. An upstream-weighted distribution of melting and thinning drives greater rates of retreat in this phase. However, greater thinning initiates faster retreat and a lagged, compensating increase in the length of the ice shelf (L_x in Eqn (20)). As noted by Parizek and Walker (2010), the increase in buttressing is principally due to lengthening of ice of a relatively constant thickness at the calving margin. After ~ 30 years, the longer ice shelf in the coupled simulation fully compensates for greater thinning-induced reductions in f_g .

Morphology-dependent melting enhances the initial decrease and subsequent increase in f_g , yet its steeper rate of increase is insufficient to slow grounding-line retreat (Fig. 6c). Any 'push' by higher grounding-line retreat rates earlier in the simulation results in larger h_g for any f_g ; if the thermal forcing remains constant, differences in the retreat rate persist over the entire integration.

The dependence of grounding-line retreat rates on glaciological setting

All the simulations listed in Table 2 show a similar temporal evolution following changes in ocean forcing (Fig. 7). The final melt rate near the grounding line is always approached within a year of an ocean perturbation. Furthermore, the temporal lag between thinning and grounding-line retreat remains similar despite substantial differences in ice-shelf morphology and grounding-line velocity. This common timescale is driven by the minimum in f_g , which occurs after ~ 10 years under a wide range of conditions, driven by compensation between the rate of retreat and the increase in f_g due to increasing length when the width parameter (Eqn (8)) is constant.

In all buttressed simulations, shearing at ice-shelf sidewalls reduces ice-shelf curvature, $\overline{\partial_{xx} h}$, relative to the unbuttressed simulations (Van der Veen, 1999, p. 169–170), moderating the along-flow gradient of coupled melt rates (and thus the magnitude of the slope wave). The influence of the coupled response on ice thickness, and its enhancement with increased thermal forcing, is more pronounced where $\overline{\partial_{xx} h}$ is larger (f_g is smaller). Since changes in melting always

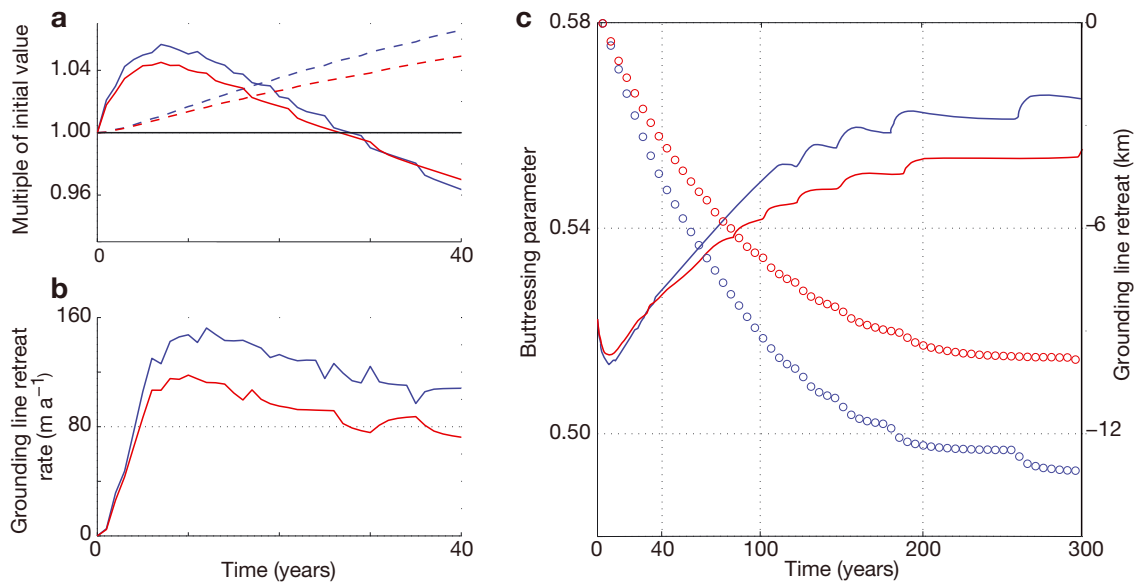


Fig. 6. The influence of a coupled melting parameterization on grounding-line retreat. The U50 coupled melting simulation is shown with blue curves and the uniform melting simulation is shown in red. In (a) the two terms of Eqn (19) are compared to their initial values following a step change in α from 0.25 to 0.50 with $(1 - f_g)^3$ as solid curves and h_g^4 as dashed curves. (b) The resulting evolution of the grounding-line retreat rate, $-\dot{x}_g$, with a 3 year averaging period. (c) The long-term behavior. The buttressing parameter, f_g (left axis, solid curves), decreases and recovers in both simulations, while the cumulative grounding-line retreat, $-\Delta x_g$ (right axis, circles), increases continuously over the first 300 years.

occur rapidly relative to grounding-line migration, we use the final melting distribution to investigate the influence of the coupled response across different ice shelves (Table 3).

Where basal curvature is positive, coupled melting distributions drive more grounding-line retreat than uniform distributions (Parizek and Walker, 2010). The impact of the distribution of melting exhibits symmetry: downstream-weighted melting results in less retreat than constant melt rates. Because increases in thickness gradients are largest near the grounding line, with successive increases in forcing, melting may transition between a downstream- and upstream-weighted distribution (Fig. 7d, U75 simulations).

The nonlinear response of ice-shelf curvature and grounding-line retreat is a function of glaciological conditions (here, bed slope and ice-stream width). As predicted by steady solutions in unbuttressed ice shelves (Appendix A), if $\overline{\partial_{xx}h} > 0$ the difference in curvature between coupled and uniform melting increases with successive step changes in α . In buttressed simulations, the difference in grounding-line retreat, $\Delta\Delta x_g$, is similarly enhanced. When bedrock is downward-sloping (e.g. the D50 simulations), successive changes in α result in enhancement of the basal curvature and larger initial decreases in f_g , yet the amount of grounding-line retreat is only slightly higher: increased thinning rates at higher α are compensated by simultaneous decreases in h_g (Eqn (19)).

DISCUSSION

Although the coupled evolution of ice-shelf morphology and basal melting prolongs the glaciological adjustment to changes in the ocean, its dynamic influence is strongly determined by the initial rapid adjustment of thickness

Table 3. Summary results for the numerical simulations. \dot{m}_{max} is the maximum basal melt rate on the domain; $\overline{\partial_{xx}h^C}$ is the spatially averaged ice-shelf curvature for the coupled simulation; $\Delta\Delta x_g$ is the difference in grounding-line retreat between the coupled and uniform melting simulations associated with the step change in thermal forcing to α . Grounding-line retreat is greater in the coupled simulation if $\Delta\Delta x_g > 0$. All other variables are defined in the text and represent the value at the final, steady state at each α

u_g km a ⁻¹	α	\dot{m}_{max} m a ⁻¹	\overline{m} m a ⁻¹	$\overline{\partial_{xx}h^C}$ 10 ⁻⁹ m ⁻¹	$\Delta\Delta x_g$ km
D00: Downward-sloping bed, $f_g(t) = 0.00$ (unbuttressed)					
5.5	0.25	35.1	8.7	3.6	0.0
5.5	0.50	108	19.9	6.2	0.0
5.5	0.75	397	35.9	18.0	0.0
U50: Upward-sloping bed, $f_g(0) = 0.50$					
2.38	0.25	9.1	4.8	1.4	0.4
2.34	0.50	27.4	9.5	2.3	2.4
	0.75			Unstable	
U75: Upward-sloping bed, $f_g(0) = 0.75$					
0.57	0.25	1.7	1.4	-0.4	-0.3
0.57	0.50	3.3	2.9	0.3	0.0
0.53	0.75	10.5	4.3	2.4	2.8
D50: Downward-sloping bed, $f_g(0) = 0.50$					
2.14	0.25	4.4	3.3	0.5	0.2
2.15	0.50	13.5	7.1	1.2	0.2
2.16	0.75	40.8	11.7	3.8	0.7
D75: Downward-sloping bed, $f_g(0) = 0.75$					
0.95	0.25	2.1	1.6	-0.8	-0.1
0.95	0.50	4.2	3.4	-0.7	-0.1
0.96	0.75	6.1	5.5	0.0	-0.1

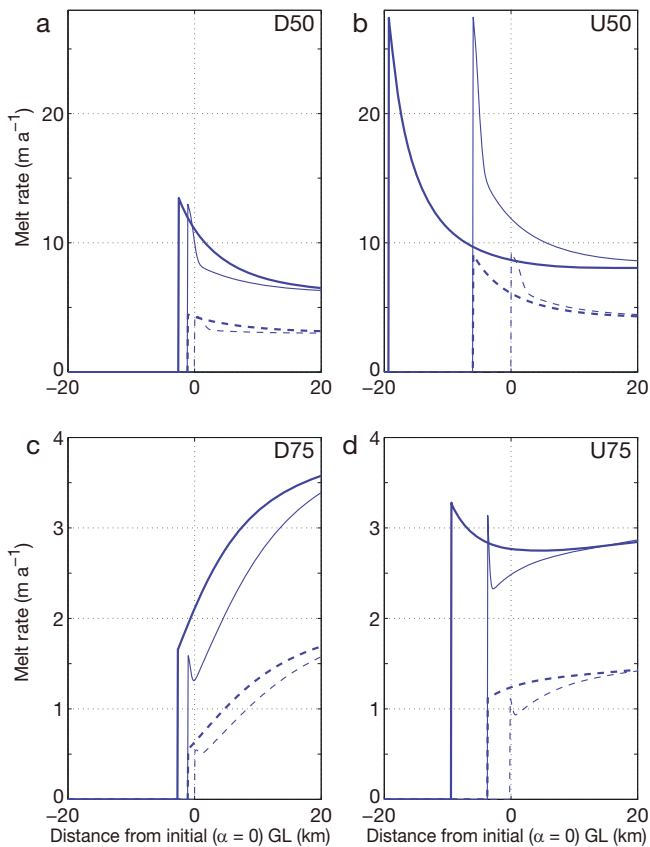


Fig. 7. Coupled melt rates in buttressed ice shelves. Each panel represents a set of two simulations with a specified bedrock slope and $f_g(0)$ (e.g. (a) shows the downward-sloping bed, $f_g(0) = 0.50$ simulations). In each panel, the local melt rate, \dot{m} , 1 year (thin curves) and 600 years (thick curves) after a step change to $\alpha = 0.25$ (dashed) and $\alpha = 0.50$ (solid) is plotted against the grounding-line position before the initiation of melting, $x_g(\alpha = 0)$. Only 20 km up- and downstream of the initial grounding-line position is shown. GL is grounding line.

gradients near grounding lines. Provided ocean forcing remains constant, melt rates remain relatively constant (as a function of distance from the grounding line) after the initial adjustment. The rapid upstream steepening that characterizes the glaciological response suggests that the key timescales described here should be qualitatively similar for a range of melt rates and distributions.

In large-scale models, representing these key aspects of the coupled response must be weighed against limits to temporal and spatial resolution. Here we discuss (1) some implications of this study for models of greater complexity and (2) the viability of the parameterizations used in these simulations, highlighting the representation of basal melting and buttressing.

Capturing rapid changes: the melting parameterization

None of these simulations attain upstream thickness gradients as large as those observed (Jenkins and others, 2010) or modeled (Joughin and others, 2010) for Pine Island Ice Shelf, Antarctica, despite the use of glaciological parameters (in the U50 simulation) derived from observations. This may result from limitations of the flowline model, errors in glaciological parameters, or poor parameterization of the melt rate. With respect to the latter, the glaciological enhancement examined here may be reinforced by the

oceanic response, described by Little and others (2009), in which n_θ in Eqn (10) is higher in steep regions. Linear increases in α also do not reflect the nonlinear sensitivity of melt rates to thermal forcing summarized by Holland and others (2008). Coupled numerical simulations using a plan-view ice model and a three-dimensional ocean model generate larger thickness gradients when compared with these simulations, principally due to stronger temperature- and slope dependence in melt rates (Goldberg, unpublished information).

In idealized ocean simulations that include a static ice shelf (e.g. Little and others, 2009), melt rates are often maximized downstream of the grounding line, where buoyancy-driven flow velocities are highest. Reduced melt rates near the grounding line – parameterized with β by Walker and others (2008) and Gagliardini and others (2010) – may be relevant to these results. However, in upstream regions, ocean dynamics may depart from those governing slope dependence (Holland, 2008). A tail-off in melt rates near the grounding line may also reflect a coupled process driven by reduced thickness gradients near the grounding line. The heightened importance of grounding zones in the coupled response suggests further effort should be devoted to understanding dominant oceanic processes in these regions. Reduced melt rates should be justified on a physical basis, rather than a function of model limitations.

These simulations indicate that melting distributions based on a common ocean parameterization depend strongly on glaciological conditions, even without complex embayment or bedrock shapes, suggesting that static (e.g. Walker and others, 2008; Pollard and DeConto, 2009; Joughin and others, 2010) and/or universal (Beckmann and Goosse, 2003) parameterizations of basal melting are of limited utility. Because the ongoing evolution of ice-shelf shape and grounding-line position do not substantially modify the melting distribution following the initial adjustment of upstream thickness gradients, a temporally fixed melting distribution might be appropriate if it is known a priori. This suggests that asynchronous coupling of a basal melting model may be sufficient to capture the relevant dynamics; however, the appropriate staggering of ocean and ice time-steps deserves further investigation. From these simulations, we infer that melt rates must be updated before significant perturbations to the stress balance result in changes to the ice-shelf morphology, and where variability in the ocean at timescales less than the ice time-step is relevant to the long-term evolution of the ice stream.

Large departures in the stress regime of ice shelves are not seen in any of these simulations, because increases in ice-shelf length compensate for thinning-induced reduction in lateral stress. Yet the significant differences in the melting distribution across simulations indicate that there is a possible rapid feedback driven by buttressing-induced shape changes if f_g decreases significantly in response to near-grounding-line thinning.

The long term: implications of longitudinal and transverse bedrock variability

A flowline model cannot represent transverse thickness or stress gradients; however, the parameterization of lateral stresses employed in these simulations compares favorably to plan-view representations of ice shelves (Goldberg and others, 2009). Simulations where lateral velocity gradients are resolved (Joughin and others, 2010) continue to un-

underscore the importance of ice-shelf thinning (and thus the advective path; MacAyeal and Barcilon, 1988) in the grounding-line response, indicating that similar processes and timescales are likely to persist in more complex models.

Perhaps more important than the details of the buttressing parameterization is its generalizability. The spatial correlation of thickness changes and the embayment shape and/or pinning points govern the influence of the form and distribution of melting. If buttressing is skewed more heavily towards the grounding line (e.g. due to changes in ice-shelf width), the distributional effects of thinning shown in Figures 4 and 5 will be more important, and the lag between thinning and grounding-line migration will be shorter. An embayment where pinning points are far from the grounding line will reverse this effect.

Though the distribution of melting resulting from the coupled response enhances grounding-line retreat in most cases, it is subject to temporal lags and requires reinforcement from glaciological factors, with implications for the initiation and persistence of enhanced grounding-line retreat rates. Increasing sensitivity to successive ocean perturbations in these simulations is a function of a short-timescale shape feedback driven by a shifting melting distribution, and a reinforcement over longer timescales driven by increasing grounding-line thickness. The role of upstream-weighted melting in these simulations may be better described as preventing a return to equilibrium in the long term, rather than initiating a dramatic short-term response. This suggests that the persistence of perturbations in the ocean and the scale of bedrock features will determine whether retreat is enhanced by the melting distribution. These time and spatial scales should be investigated with more complete representations of bedrock topography and oceanic variability.

Our simulations contradict the assumption that ice shelves evolve slowly. Although transient changes in ocean forcing are not explored in this study, the rapid ice thickness evolution also implies that short-term, localized changes may affect grounding-line migration long after an oceanic perturbation. The importance of these considerations is heightened if the advected signal is important to buttressing. The preservation of melting perturbations and the embayment shape will determine whether short-timescale changes in ocean forcing (<months) must be represented in longer model integrations.

The role of calving and far-field buttressing

Increases in buttressing driven by a lengthening ice shelf can limit the short-term influence of thinning and long-term influence of changes in grounding-line driving stress (Fig. 6; Appendix B). However, assuming that the ice-shelf length is only affected by changes in the position of the grounding line (and not the calving front) may underestimate the impact of the basal melting distribution. Though calving is difficult to parameterize (Van der Veen, 2002; Benn and others, 2007), its importance is evident in simulations (Fig. 8) where buttressing is removed as the grounding line retreats, e.g.

$$\tau_y(x > x_g + L_x(t = 0)) = 0 \quad (21)$$

Without greater lateral stresses derived from the far field, an ice shelf that is thicker on an area-average basis is insufficient to counteract retreat; changes in driving stress dominate, leading to accelerating, unstable retreat within decades of a change in ocean forcing. In these simulations, ice streams

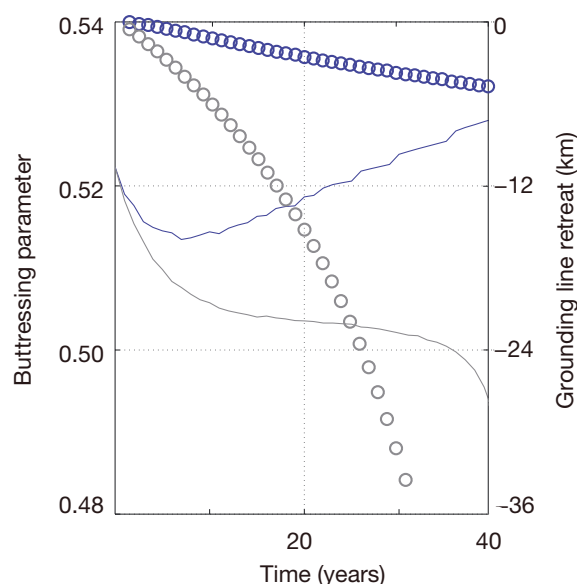


Fig. 8. The influence of a retreating calving front. Gray symbols show the evolution of the buttressing parameter, f_g (left axis, solid curves), and cumulative grounding-line retreat, $-\Delta x_g$ (right axis, circles), using the alternate buttressing parameterization described by Eqn (21). Blue lines and circles are identical to those in the U50 simulation shown in Figure 6c.

that deepen inland are unstable even when subject to small melting perturbations.

The processes associated with migration of the calving front, and their overlap with the coupled response to melting, are complex. Previous studies suggest that inland perturbations are dominated by calving/break-up events, but that melting preconditions ice shelves (Glasser and Scambos, 2008; Sole and others, 2008). It is not clear how the coupled response might influence calving, as reduced longitudinal stresses under thinner ice shelves give lower calving rates in simple calving laws (Alley and others, 2008). The distribution of melting may influence calving indirectly via its influence on ice temperature and rheology (Khazendar and others, 2007; Holland and others, 2009). The coupling of the melting distribution and calving, the importance of far-field buttressing and calving parameterizations (or the lack of one) should be critically assessed for their effect on grounding-line retreat rates.

CONCLUSIONS

Using numerical simulations of an ice-shelf/ice-stream system with a simple basal melting parameterization, we have investigated the processes and timescales governing the coupled ice/ocean response to perturbations in ocean temperature. When ice-shelf basal melt rates are morphology-dependent, the melting distribution is coupled to the evolving stress state of the ice-shelf/ice-stream system, and grounding-line retreat rates are a function of that distribution. Here we find that, following a rapid adjustment to changed ocean forcing in upstream regions of the ice shelf, coupled melt rates remain relatively constant with distance from the grounding line. The difference in grounding-line retreat rates between morphology-dependent and spatially uniform melting (with the same average melt rate) is driven by the distribution established after the initial adjustment.

The difference is enhanced if the shape of the ice shelf – driven by bedrock morphology and embayment width – acts to concentrate melting upstream. Because the distribution of melting shifts upstream with successive increases in forcing, the coupled response drives a nonlinear relationship between ocean forcing and grounding-line retreat.

In these simulations, decreases in the sidewall area of the ice shelf dominate reductions in lateral stress that, in turn, increase the rate of grounding-line retreat. Differences in the melting distribution have a limited effect until upstream thinning is integrated by ice flow. As thinning propagates through the ice shelf, upstream-weighted (downstream-weighted) melting distributions drive faster (slower) grounding-line retreat rates than spatially uniform melting. Extension of the ice shelf strongly compensates for differences in retreat rates driven by melting-induced thinning. After a time approximately equal to the advective timescale of the ice shelf, bed morphology becomes the principal control on the rate of retreat. If the bed deepens with retreat, initially higher rates of retreat due to upstream-weighted melting persist over the long term (centuries).

Large-scale coupled models will be required to adequately resolve the rapid adjustment to changed ocean conditions in upstream regions of ice shelves. Further efforts to clarify this relationship should be directed toward (1) modeling ice shelves with a two-dimensional representation of lateral stresses and longitudinally varying embayment widths, (2) determining whether generalized forms of buttressing are viable and (3) understanding the interaction between melting and calving.

ACKNOWLEDGEMENTS

We thank Olga Sergienko for valuable suggestions at several stages during the evolution of the manuscript. The comments of two anonymous reviewers and the editor greatly improved its clarity. C.M.L. is grateful for financial support from the Carbon Mitigation Initiative in the Princeton Environmental Institute and the Science, Technology and Environmental Policy program in the Woodrow Wilson School of Public and International Affairs at Princeton University.

REFERENCES

- Alley RB and 7 others (2008) A simple law for ice-shelf calving. *Science*, **322**(5906), 1344 (doi: 10.1126/science.1162543)
- Beckmann A and Goosse H (2003) A parameterization of ice shelf–ocean interaction for climate models. *Ocean Model.*, **5**(2), 157–170
- Benn DI, Warren CR and Mottram RH (2007) Calving processes and the dynamics of calving glaciers. *Earth-Sci. Rev.*, **82**(3–4), 143–179.
- Dupont TK (2004) Abrupt changes in ice shelves and ice streams: model studies. (PhD thesis, Pennsylvania State University)
- Dupont TK and Alley RB (2005) Assessment of the importance of ice-shelf buttressing to ice-sheet flow. *Geophys. Res. Lett.*, **32**(4), L04503 (doi: 10.1029/2004GL022024)
- Gagliardini O, Durand G, Zwinger T, Hindmarsh RCA and Le Meur E (2010) Coupling of ice-shelf melting and buttressing is a key process in ice-sheets dynamics. *Geophys. Res. Lett.*, **37**(14), L14501 (doi: 10.1029/2010GL043334)
- Glasser NF and Scambos TA (2008) A structural glaciological analysis of the 2002 Larsen B ice-shelf collapse. *J. Glaciol.*, **54**(184), 3–16
- Goldberg DN, Holland DM and Schoof CG (2009) Grounding line movement and ice shelf buttressing in marine ice sheets. *J. Geophys. Res.*, **114**(F4), F04026 (doi: 10.1029/2008JF001227)
- Holland DM and Jenkins A (1999) Modeling thermodynamic ice ocean interactions at the base of an ice shelf. *J. Phys. Oceanogr.*, **29**(8), 1787–1800
- Holland PR (2008) A model of tidally dominated ocean processes near ice shelf grounding lines. *J. Geophys. Res.*, **113**(C11), C11002 (doi: 10.1029/2007JC004576)
- Holland PR, Jenkins A, Holland DM (2008) The response of ice shelf basal melting to variations in ocean temperature. *J. Climate*, **21**(11), 2558–2572
- Holland PR, Corr HFJ, Vaughan DG, Jenkins A and Skvarca P (2009) Marine ice in Larsen Ice Shelf. *Geophys. Res. Lett.*, **36**(11), L11604 (doi: 10.1029/2009GL038162)
- Jacobs SS, Hellmer HH and Jenkins A (1996) Antarctic ice sheet melting in the southeast Pacific. *Geophys. Res. Lett.*, **23**(9), 957–960
- Jacobs SS, Jenkins A, Giulivi CF and Dutrieux P (2011) Stronger ocean circulation and increased melting under Pine Island Glacier ice shelf. *Nature Geosci.*, **4**(8), 519–523
- Jenkins A and 6 others (2010) Observations beneath Pine Island Glacier in West Antarctica and implications for its retreat. *Nature Geosci.*, **3**(7), 468–472
- Joughin I, Smith BE, Holland DM (2010) Sensitivity of 21st century sea level to ocean-induced thinning of Pine Island Glacier, Antarctica. *Geophys. Res. Lett.*, **37**(20), L20502 (doi: 10.1029/2010GL044819)
- Khazendar A, Rignot E and Larour E (2007) Larsen B Ice Shelf rheology preceding its disintegration inferred by a control method. *Geophys. Res. Lett.*, **34**(19), L19503 (doi: 10.1029/2007GL030980)
- Little CM, Gnanadesikan A and Oppenheimer M (2009) How ice shelf morphology controls basal melting. *J. Geophys. Res.*, **114**(C12), C12007 (doi: 10.1029/2008JC005197)
- MacAyeal DR (1989) Large-scale ice flow over a viscous basal sediment: theory and application to Ice Stream B, Antarctica. *J. Geophys. Res.*, **94**(B4), 4071–4087
- MacAyeal DR and Barcilon V (1988) Ice-shelf response to ice-stream discharge fluctuations: I. Unconfined ice tongues. *J. Glaciol.*, **34**(116), 121–127
- MacAyeal DR and Lange MA (1988) Ice-shelf response to ice-stream discharge fluctuations: II. Ideal rectangular ice shelf. *J. Glaciol.*, **34**(116), 128–135
- Nick FM, Vieli A, Howat IM and Joughin I (2009) Large-scale changes in Greenland outlet glacier dynamics triggered at the terminus. *Nature Geosci.*, **2**(2), 110–114
- Parizek BR and Walker RT (2010) Implications of initial conditions and ice–ocean coupling for grounding-line evolution. *Earth Planet. Sci. Lett.*, **300**(3–4), 351–358
- Paterson WSB (1994) *The physics of glaciers*, 3rd edn. Elsevier, Oxford
- Payne AJ, Vieli A, Shepherd A, Wingham DJ and Rignot E (2004) Recent dramatic thinning of largest West Antarctic ice stream triggered by oceans. *Geophys. Res. Lett.*, **31**(23), L23401 (doi: 10.1029/2004GL021284)
- Pollard D and DeConto RM (2009) Modelling West Antarctic ice sheet growth and collapse through the past five million years. *Nature*, **458**(7236), 329–332
- Pritchard HD, Arthern RJ, Vaughan DG and Edwards LA (2009) Extensive dynamic thinning on the margins of the Greenland and Antarctic ice sheets. *Nature*, **461**(7266), 971–975 (doi: 10.1038/nature08471)
- Rignot E (2008) Changes in West Antarctic ice stream dynamics observed with ALOS PALSAR data. *Geophys. Res. Lett.*, **35**(12), L12505 (doi: 10.1029/2008GL033365)
- Rignot E and Jacobs SS (2002) Rapid bottom melting widespread near Antarctic ice sheet grounding lines. *Science*, **296**(5575), 2020–2023

Rignot E and 6 others (2008) Recent Antarctic ice mass loss from radar interferometry and regional climate modelling. *Nature Geosci.*, **1**(2), 106–110

Schmeltz M, Rignot E, Dupont TK and MacAyeal DR (2002) Sensitivity of Pine Island Glacier, West Antarctica, to changes in ice-shelf and basal conditions: a model study. *J. Glaciol.*, **48**(163), 552–558

Schoof C (2007) Marine ice-sheet dynamics. Part 1. The case of rapid sliding. *J. Fluid Mech.*, **573**, 27–55

Scott JBT, Gudmundsson GH, Smith AM, Bingham RG, Pritchard HD and Vaughan DG (2009) Increased rate of acceleration on Pine Island Glacier is strongly coupled to thinning induced changes in driving stress. *Cryosphere*, **3**(1), 125–131

Shepherd A and Wingham D (2007) Recent sea-level contributions of the Antarctic and Greenland ice sheets. *Science*, **315**(5818), 1529–1532

Sole A, Payne T, Bamber J, Nienow P and Krabill W (2008) Testing hypotheses of the cause of peripheral thinning of the Greenland Ice Sheet: is land-terminating ice thinning at anomalously high rates? *Cryosphere*, **2**(2), 205–218

Thoma M, Jenkins A, Holland D and Jacobs S (2008) Modelling circumpolar deep water intrusions on the Amundsen Sea continental shelf, Antarctica. *Geophys. Res. Lett.*, **35**(18), L18602 (doi: 10.1029/2008GL034939)

Thomas R (2004) Force-perturbation analysis of recent thinning and acceleration of Jakobshavn Isbrae, Greenland. *J. Glaciol.*, **50**(168), 57–66.

Van der Veen CJ (1999) *Fundamentals of glacier dynamics*. AA Balkema, Rotterdam

Van der Veen CJ (2002) Calving glaciers. *Progr. Phys. Geogr.*, **26**(1), 96–122

Vaughan DG and 9 others (2006) New boundary conditions for the West Antarctic ice sheet: subglacial topography beneath Pine Island Glacier. *Geophys. Res. Lett.*, **33**(9), L09501 (doi: 10.1029/2005GL025588)

Walker RT and Holland DM (2007) A two-dimensional coupled model for ice shelf–ocean interaction. *Ocean Model.*, **17**(2), 123–139

Walker RT, Dupont TK, Parizek BR and Alley RB (2008) Effects of basal-melting distribution on the retreat of ice-shelf grounding lines. *Geophys. Res. Lett.*, **35**(17), L17503 (doi: 10.1029/2008GL034947)

Wingham DJ, Wallis DW and Shepherd A (2009) Spatial and temporal evolution of Pine Island Glacier thinning, 1995–2006. *Geophys. Res. Lett.*, **36**(17), L17501 (doi: 10.1029/2009GL039126)

Wu XM and 8 others (2010) Simultaneous estimation of global present-day water transport and glacial isostatic adjustment. *Nature Geosci.*, **3**(9), 642–646

Zwally HJ and Giovinetto MB (2011) Overview and assessment of Antarctic ice-sheet mass balance estimates: 1992–2009. *Surv. Geophys.*, **32**(4–5), 351–376

APPENDIX A: A STEADY-STATE ICE TONGUE WITH LINEARLY SLOPE-DEPENDENT MELTING

In a steady state, Eqn (3) becomes

$$\frac{d(uh)}{dx} = -\dot{m} \tag{A1}$$

Combining Eqns (A1) and (14):

$$\frac{dh}{dx} = -\frac{\dot{m} + \left[\frac{\rho_i g}{4} \left(1 - \frac{\rho_i}{\rho_w} \right) \right]^n Ah^{n+1}}{u} \tag{A2}$$

Analogous to Van der Veen’s (1999) technique for an ice shelf with constant accumulation, we integrate Eqn (A1):

$$uh = u_g h_g - \int_{x_g}^x \dot{m} dx \tag{A3}$$

Substituting Eqns (A3) and (11) into Eqn (A2) gives

$$\frac{dh}{dx} = -\frac{\left[\frac{\rho_i g}{4} \left(1 - \frac{\rho_i}{\rho_w} \right) \right]^n Ah^{n+2}}{u_g h_g (1 - \alpha)} \tag{A4}$$

In a steady one-dimensional ice tongue, where $\frac{du}{dx} > 0$, $0 \leq \alpha < 1$. If $\alpha \geq 1$, the specified ice flux is not sufficient to counter melting at the grounding line (Eqn (A1)). Integrating Eqn (A4) from $x = 0$, where $h = h_g$:

$$\frac{h(x)}{h_g} = \left\{ \frac{(n+1) \left[\frac{\rho_i g}{4} \left(1 - \frac{\rho_i}{\rho_w} \right) \right]^n Ah_g^n}{u_g (1 - \alpha)} x + 1 \right\}^{-\frac{1}{n+1}} \tag{A5}$$

Except for the presence of α , Eqn (A5) is identical to eqn (6.6.8) of Van der Veen (1999).

The local sensitivity to α

Equation (A5) can be rewritten

$$\frac{h(x)}{h_g} = \left(1 + \frac{x}{l} \right)^{-\frac{1}{n+1}} \tag{A6}$$

where

$$l = \frac{1}{(n+1)} \left[\frac{\rho_i g}{4} \left(1 - \frac{\rho_i}{\rho_w} \right) \right]^{-n} \frac{u_g (1 - \alpha)}{Ah_g^n} \tag{A7}$$

A single length scale, l , controls the distance from the grounding line over which ice shelves steepen in response to a change in oceanic forcing or glaciological parameters. In an ice tongue with slope-dependent melting, thickness gradients (and melt rates) are highest at the grounding line and decrease monotonically downstream,

$$\frac{dh}{dx} = -\frac{h_g}{(n+1)l} \left(1 + \frac{x}{l} \right)^{-\frac{n+2}{n+1}} \tag{A8}$$

The local sensitivity of the ice thickness gradient is given by

$$\frac{d^2 h}{dx dl} = h_g \left[\frac{\left(1 + \frac{x}{l} \right)^{-\frac{n+2}{n+1}}}{(n+1)l^2} - \frac{(n+2)x \left(1 + \frac{x}{l} \right)^{-\frac{2n+3}{n+1}}}{(n+1)^2 l^3} \right] \tag{A9}$$

Increases in α increase thickness gradients where $x > (n+1)l$. With the parameters used in these simulations, virtually all of the ice shelf steepens with increasing α ; the largest increases occur at the grounding line (Fig. 9a). Increases in α always increase the mean curvature, $(d^2 h/dx^2)$, shifting the distribution of melting upstream, and reducing the cross-sectional area at any x (Fig. 9b).

Determination of the average melt rate

Solutions to Eqn (A5) require an arbitrary ‘calving’ criterion, with implications for the area-average melt rate, given by

$$\bar{m} = \frac{\int_{x_g}^{x_c} \dot{m} dx}{x_c - x_g} = \frac{\alpha u_g (h_v g - h_c)}{L_x} \tag{A10}$$

where x_c is the implied location of the calving front and the ice-shelf length is $L_x = x_c - x_g$.

If x_c is sufficiently far from the grounding line (e.g. $\frac{dh}{dx}|_{x_c} \Rightarrow 0$), then \bar{m} increases linearly with thermal forcing. Linear increases in spatially averaged melt rates are driven primarily by nonlinear increases in melt rates and basal slopes near the grounding line.

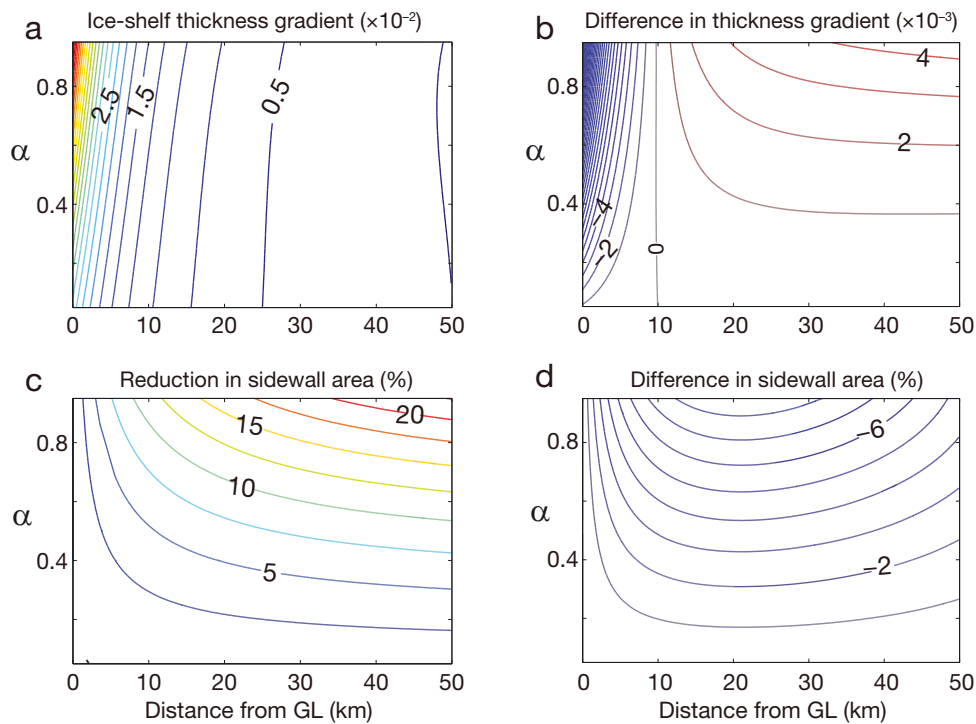


Fig. 9. The morphological influence of basal melting (Eqn (11)) in a steady ice tongue (Eqn (A5)). The left column shows (a) the logarithm of the ice thickness gradient ($\log_{10} \left| \frac{dh}{dx} \right|$) within 50 km of the grounding line and (c) the percent reduction in sidewall area, from a solution with $\alpha = 0$. In the right column, morphological differences between steady solutions for coupled and uniform basal melting are compared at different ocean forcing, α . (b) Differences in the local ice thickness gradient; negative values indicate the coupled solution is steeper. (d) The additional reduction in running mean ice thickness due to the coupled melting distribution at each point along the ice shelf. Parameters in Eqn (A5) are those in Table 1; $u_g = 5500 \text{ m a}^{-1}$ and $h_g = 950 \text{ m}$. GL is grounding line.

Comparison to uniform melting

Because an ice shelf with slope-dependent melting is steeper near the grounding line (Fig. 9b), it is thinner on a spatially averaged basis than an ice shelf with the same spatially averaged melt rate (Fig. 9d). The change in sidewall area of the ice shelf is a function of the distribution of thickness changes, and is larger for slope-dependent melting at all points along the ice shelf. With increasing α , differences in sidewall area between coupled and uniform melting distributions increase, although the exact rate of increase is a function of position along the ice shelf.

The morphological impact of slope-dependent melting is heightened when x_c is larger, yet qualitative results shown in Figure 9 are insensitive to this choice.

APPENDIX B: ICE-SHELF CONTROL OF GROUNDING-LINE RETREAT

Insight into the timing and controls of grounding-line retreat can be provided by the total derivative of Eqn (5):

$$-\dot{x}_g = \frac{u_g \partial_x h + h_g \partial_x u}{\partial_x h + \frac{\rho_w}{\rho_i} \partial_x z_{\text{bed}}} \quad (\text{B1})$$

where $\dot{m} = 0$ at the grounding line. Eqn (B1) is appropriate where longitudinal stress on the grounded ice is asymptotically small when compared with basal friction (appendix A of Schoof, 2007). Under these conditions, a boundary layer is not required to match fluxes between grounded and floating ice (Schoof, 2007). The three terms in Eqn (B1) describe (1) thickness advection, $u_g \partial_x h < 0$, (2) longitudinal stress, or stretching, $h_g \partial_x u > 0$, and (3) the

local gradient of the bottom pressure (the denominator), which moderates the rate of retreat. Using Eqns (1), (5) and (9), $\partial_x u$ can be related to f_g , giving

$$-\dot{x}_g = \frac{u_g \partial_x h + \left[\frac{\rho_i g}{4} \left(1 - \frac{\rho_i}{\rho_w} \right) \right]^n A h_g^{n+1} (1 - f_g)^n}{\partial_x h + \frac{\rho_w}{\rho_i} \partial_x z_{\text{bed}}} \quad (\text{B2})$$

In Figure 10a, we compare the evolution of the individual terms in Eqn (B2). Although only the U50 simulation is shown, the dominance of the stretching term is common across the simulations performed here. Following the initiation of melting, increases in thickness and velocity gradients drive increases in the magnitude of all three terms. However, changes in stretching (black solid curve), driven by changes in ice-shelf morphology, are only partially compensated by transient increases in the grounding-line velocity and slope, and the grounding line retreats. The advective flux from the ice stream (gray dashed curve) requires almost a century to balance changes in stretching and does not play a dominant role in re-equilibration to changed melt rates; an increase in f_g allows the grounding line to stabilize, despite a decrease in grounding-line velocity and a relaxation in the ice thickness gradient.

In Figure 10b, selected components of the stretching term are held constant, illuminating their importance. By fixing the ice-shelf velocity ($u = u(t = 0)$, dashed gray curve), the weak influence of velocity changes in the short term is apparent. Comparison with the unapproximated term (black solid curve) indicates that f_g is controlled by changes in the sidewall area until changes in u_g driven by grounding-line

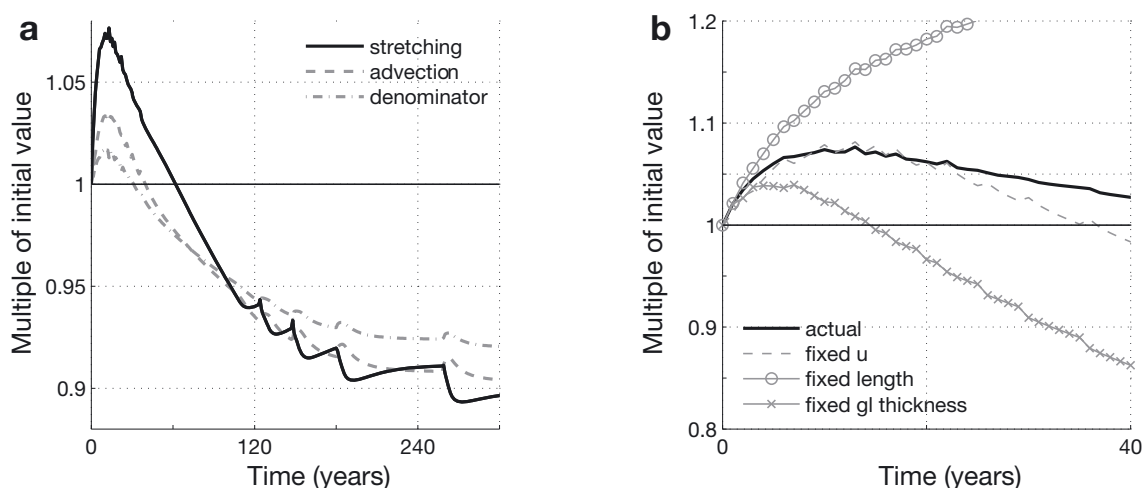


Fig. 10. Time evolution of controls on grounding-line migration. (a) The three terms of Eqn (B2) in the U50 coupled simulation compared to their initial values. Increases in stretching (black solid curve) that are not compensated by advection from upstream (gray dashed curve) drive faster grounding-line retreat rates, with some moderation by the denominator (gray dash-dot curve). Jumps in the values of all quantities are caused by discretization of the output. (b) Validity of various approximations (gray curves, described in the text) to the stretching term in Eqn (B2) (black curve, identical to that in (a)) is compared over the first 40 years of the same simulation. GL is grounding line.

migration become relevant (after year 20). By eliminating buttressing derived from extension of the ice shelf ($L_x(t) = L_x(t = 0)$, gray circles), thin regions of the ice shelf near calving margins are revealed to be critical to the increase in buttressing. The final approximation in Figure 10b isolates the influence of bed topography ($h_g = h_g(t = 0)$, gray crosses). For approximately the first decade, all the curves

in Figure 10b lie close to each other; the reduction of buttressing through thinning dominates the grounding-line retreat. Following this period, the grounding-line evolution is determined by compensation between ice-shelf length and grounding-line depth (which increases with retreat); the final grounding-line position is principally a function of bedrock topography.

MS received 6 March 2011 and accepted in revised form 13 October 2011